NANO LETTERS

Letter

pubs.acs.org/NanoLett

Correlating Catalytic Activity of Ag−Au Nanoparticles with 3D Compositional Variations

Thomas J. A. Slater,[†] Alexandra Macedo,[‡] Sven L. M. Schroeder,[§,∥] M. Grace Burke,[†] Paul O'Brien,[†,∥] Pedro H. C. Camargo,*[,‡] and Sarah J. Haigh*[,†]

[†]School of Materials, The University of Manchester, Manchester, M13 9PL, United Kingdom

[‡]Departamento de Química Fundamental, Instituto de Química, Universidade de São Paulo, São Paulo 05508-000, Brazil

[§]School of Chemical Engineering and Analytical Science, The University of Manchester, Manchester, M13 9PL, United Kingdom

[∥]School of Chemistry, The University of Manchester, Manchester, M13 9PL, United Kingdom

Supporting Information

ABSTRACT: Significant elemental segregation is shown to exist within individual hollow silver−gold (Ag−Au) bimetallic nanoparticles obtained from the galvanic reaction between Ag particles and $AuCl_4^-$. Three-dimensional compositional mapping using energy dispersive X-ray (EDX) tomography within the scanning transmission electron microscope (STEM) reveals that nanoparticle surface segregation inverts from Au-rich to Ag-rich as Au content increases. Maximum Au surface coverage was observed for nanoparticles with approximately 25 atom % Au, which correlates to the optimal catalytic performance in a three-component coupling reaction among cyclohexane carboxyaldehyde, piperidine, and phenylacetylene.

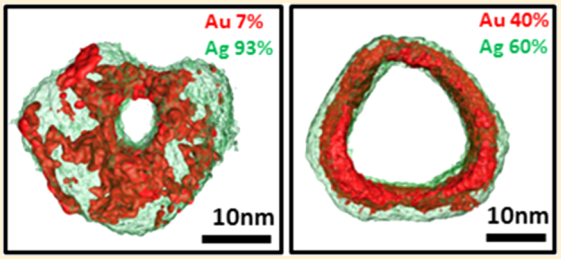

KEYWORDS: *Galvanic replacement reaction, hollow bimetallic nanoparticles, heterogeneous catalysis, scanning transmission electron microscopy, energy dispersive X-ray spectroscopy, electron tomography*

The exceptional catalytic properties of Au nanoparticles as compared to the inert nature of the bulk element are well-known.[1] The emergence of catalytic activity as particles' critical dimensions approach nanometer scale is in part due to the increase in the particle's surface-to-volume ratio.[1] Synthetic routes that maximize this property, especially in distinct geometries such as hollow shells or cages,[2,3] have been extensively investigated. Bimetallic noble metal nanoparticles are known to have excellent catalytic performance in a wide range of reactions.[4] The extent of alloying in these systems is known to influence catalytic activity and selectivity, but an understanding of the origin of this effect is lacking.[5] Hollow bimetallic nanoparticles of accurately tunable size, shape, and composition can be readily prepared by a galvanic replacement reaction.[6−8] The Ag−Au bimetallic system offers the opportunity to both reduce the cost of the Au catalysts and enhance catalytic performance.[9,10] Hollow Ag−Au nanostructures of various compositions and shapes have been synthesized by galvanic reactions between Au metal salts, such as $AuCl_4^-$, and Ag nanoparticle sacrificial templates.[10,11] Previous low-resolution transmission electron microscope (TEM) imaging and optical spectroscopy observations suggest that this process initiates with the creation of Ag ions at the surface and the formation of a gold surface layer which immediately transforms into an Au−Ag alloy because of the fast interdiffusion between gold and silver at 100 °C.[7,12] As the replacement reaction proceeds, dealloying and processes such as Ostwald ripening induce morphological reconstruction, as well as the formation, and enlargement, of pinholes in the walls. However, the alloying in individual particles, as well as the effect of elemental segregation on catalytic properties, was previously unknown. Details of elemental distribution have now been made clear by analytical EDX analysis within the STEM that has only become possible due to recent advances in EDX detector design.

Ag−Au nanoparticles with controlled compositions and structures (solid vs hollow interiors) were synthesized by the galvanic replacement reaction between Ag nanoparticles and different amounts of $AuCl_4^-$. The average compositions as determined by flame atomic absorbance spectrometry were $Ag_{93}Au_7$, $Ag_{82}Au_{18}$, $Ag_{78}Au_{22}$, and $Ag_{66}Au_{34}$. The catalytic activity of the Ag−Au nanoparticles as a function of composition and structure was investigated for the three-component (A^3) coupling reaction among cyclohexanecarboxyaldehyde, piperidine, and phenylacetylene to form propargylamines (Figure 1a). Propargylamines are useful intermediates in the synthesis of heterocyclic compounds and represent structural elements of several natural products and drugs, which has led to their use as intermediates in the total synthesis of such molecules.[13,14] Recently, it has been shown that this transformation can be catalyzed by nanostructured Au via a C−

Received: December 20, 2013
Revised: February 24, 2014
Published: February 28, 2014

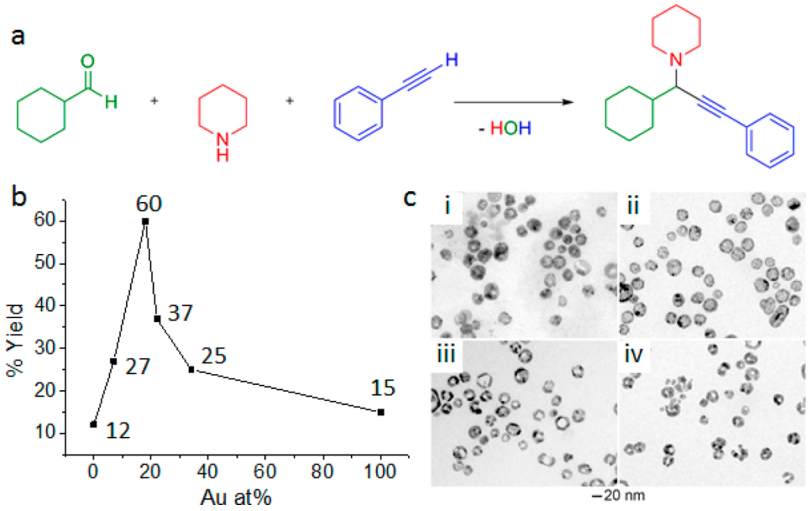

Figure 1. Ag–Au bimetallic nanoparticles improve propargylamine yield. (a) Three-component coupling reaction to form propargylamines. (b) Propargylamine yield as a function of the composition of the nanoparticle catalysts demonstrating a spike in yield for an average composition of 18 atom % Au (numerical percentage yields are noted on the graph). (c) TEM images of the synthesized Ag–Au nanoparticles with labels corresponding to the average bimetallic compositions plotted in b, (i) $Ag_{93}Au_7$, (ii) $Ag_{82}Au_{18}$, (iii) $Ag_{78}Au_{22}$, and (iv) $Ag_{66}Au_{34}$.

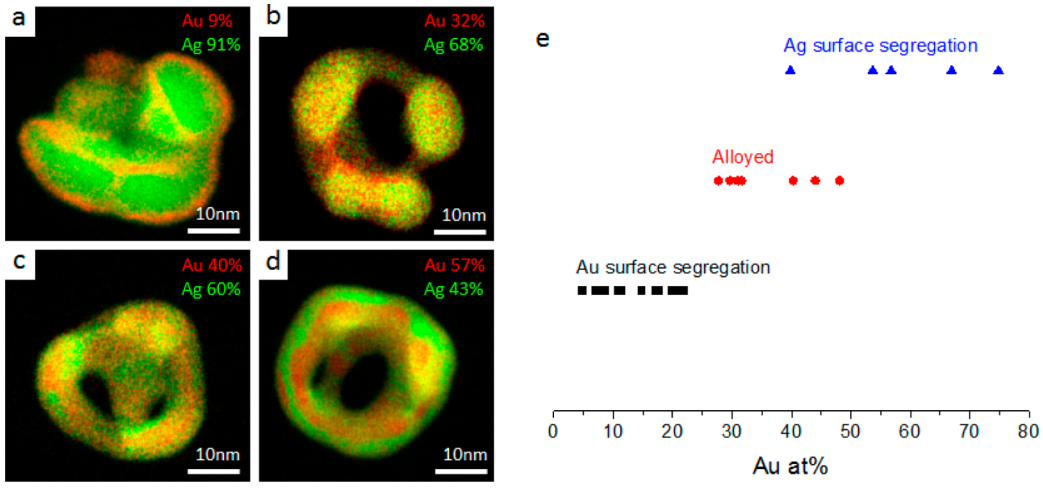

Figure 2. STEM EDX mapping showing the inversion of surface segregation behavior for Ag–Au nanoparticles as the Au content is increased. EDX maps for representative nanoparticles from populations with average stoichiometry (a) $Ag_{93}Au_7$, (b) $Ag_{82}Au_{18}$, (c) $Ag_{78}Au_{22}$, and (d) $Ag_{66}Au_{34}$. The actual composition of each nanoparticle shown inset was measured using the summed EDX spectrum for the whole field of view of each spectrum image. The chemistry of 20 nanoparticles with a range of compositions was mapped and the structure classified as to whether the particle appeared to show a gold-rich surface, a silver-rich surface, or no surface segregation (alloyed composition). The average nanoparticle composition was then measured from the summed spectral image, and the results are shown in e. The change from gold to silver surface segregation is found to correlate with the gold content of the nanoparticle.

H activation mechanism.[15,16] The yield of propargylamines as a function of the Au atomic percentage in the Ag–Au nanoparticles is given in Figure 1b. All of the bimetallic and hollow Ag–Au nanoparticles produce higher yields of propargylamine than their solid and monometallic counterparts (Ag or Au nanoparticles). This observation could be related to a change in electronic structure on account of the bimetallic composition or to the increased surface area due to the formation of hollow interiors as shown in the TEM images (Figure 1c).

More surprising is an exceptionally high peak in yield of 60% at a catalyst composition of 18 at. % Au (Figure 1b). TEM imaging shows that the sizes and morphologies of the nanoparticles are broadly similar for all bimetallic compositions (Figure 1c), suggesting that the observed peak in the catalytic results is not explained by size, shape, or surface area differences alone.

Nanoscale compositional variations have been observed to strongly affect the catalytic activity of platinum (Pt) alloy nanoparticles.[17,18] Au and Ag form a miscible solid solution over the full range of compositions; the lattice parameter of Au is just 0.2% larger than that of Ag. Therefore, structurally sensitive techniques, such as X-ray diffraction, electron diffraction, and high resolution TEM imaging, are unable to distinguish among monometallic, alloyed, or composite nanoparticles in the Ag–Au system. UV–visible spectroscopy[19,20] and X-ray photoelectron spectroscopy (XPS)[20] have been used to elucidate surface composition for bimetallic nanoparticles but cannot provide information on the local distribution of elements or on the variation of alloying inside the volume of a nanoparticle. XPS data for our system suggests an enhancement

dx.doi.org/10.1021/nl4047448 | Nano Lett. 2014, 14, 1921–1926

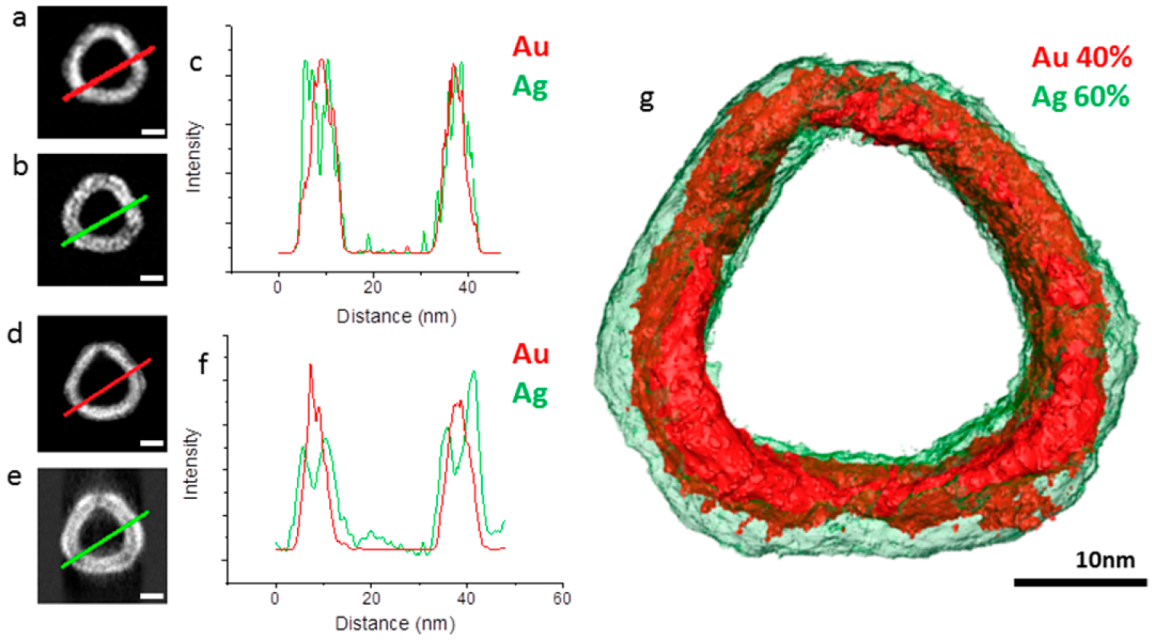

Figure 3. 3D chemical mapping of an Ag−Au nanoparticle with a high Au content showing Ag surface segregation. Two-dimensional EDX maps acquired at zero degrees of tilt showing the distribution of (a) Au and (b) Ag. (c) Compositional variation extracted right to left from the 2D maps at the position of the line shown in a and b. 2D EDX maps extracted from the 3D tomograms showing the distribution of (d) Au and (e) Ag. (f) Compositional variation extracted right to left from the 2D slices shown in d and e. The line profile extracted from the tomographic data slice more clearly reveals the silver surface segregation due to the improved resolution in the *z* direction. (g) Surface visualization of the Au (red) and Ag (green) tomograms revealing the silver surface segregation (see Supporting Movie S1). The average composition measured for the whole nanoparticle is given inset. The scale bars in a, b, d, and e are 10 nm.

in Au composition at the surface which decreases as the total Au content increases up to 34 at. % (see Supporting Information), but the polydispersity of the population makes deeper interpretation difficult. High-angle annular dark-field (HAADF) scanning transmission electron microscope (STEM) imaging is able to reveal local compositional variation if there are sufficiently large differences in the average atomic number of constituent elements. However, the nonuniform cross section of our particles meant that HAADF STEM imaging of the nanoparticles in this study was inconclusive (Supporting Information Figure S1a).

Through the combination of STEM imaging with electron energy loss (EEL) or EDX spectroscopy, it is possible to obtain chemical information with a spatial resolution that approaches 0.1 nm for bulk oxides.[21,22] Using high efficiency EDX spectroscopy, coupled with aberration corrected STEM imaging, high-resolution chemical spectrum images for >20 of the Ag−Au bimetallic nanoparticles of different compositions were obtained (Figure 2). These images are the first observation of a reversal in the surface segregation within individual nanoparticles with increased Au content. Nanoparticles with a low Au content (average composition $Ag_{93}Au_7$) have an approximately 1 nm Au-rich surface layer, whereas many particles from the sample with the highest Au concentration (average composition $Ag_{66}Au_{34}$) exhibited Ag surface segregation. Nanoparticles of intermediate average composition $Ag_{82}Au_{18}$ displayed mixed segregation; most appeared homogeneous in composition but a small fraction (~20%) showed an Au-rich surface layer. Nanoparticles with intermediate average composition $Ag_{78}Au_{22}$ were also mostly homogeneously alloyed except for a small fraction that displayed Ag surface segregation. The apparent surface segregation behavior for an individual nanoparticle correlates well with its actual Au composition measured by processing the EDX sum spectra obtained over the entire field-of-view for each spectrum image (Figure 2e). To gain a better understanding of the surface segregation behavior, line profiles have been extracted perpendicular to the surface of the elemental maps (Figure 2a−d). Such two-dimensional elemental images can be difficult to interpret because different compositions overlap when projected along the electron beam direction. For example, Figure 3c shows a line compositional profile extracted from the 2D elemental maps in Figure 3a,b in which Ag appears to be clearly segregated to the surfaces for the left-hand side of the nanoparticle ring but not for the right-hand side.

STEM imaging can be extended to provide three-dimensional information through electron tomography, in which two-dimensional images are acquired at a range of sample tilts in a method similar to X-ray tomography. Electron tomography using HAADF STEM imaging has proven a useful tool in the analysis of nanoparticle size, shape, and distribution.[23] Energy filtered transmission electron microscopy (EFTEM)[24] and STEM imaging with EDX spectroscopy[24,25] can provide chemical sensitivity to electron tomographic reconstructions, but both approaches are challenging. New EDX detector designs (see Supporting Information) combined with the increased currents and small probe size obtainable in aberration corrected STEM instruments mean that EDX tomography is now an increasingly viable tool for nanoparticle characterization.

To better understand the surface segregation behavior of the nanoparticles, EDX tomograms were compared for a nanoparticle exhibiting Ag-surface segregation with another showing evidence of Au-rich surface segregation. The Ag surface-segregated nanoparticle reveals a fairly uniform surface layer approximately 2 nm thick (Figure 3d,e). The compositional line

dx.doi.org/10.1021/nl4047448 | *Nano Lett.* 2014, 14, 1921−1926

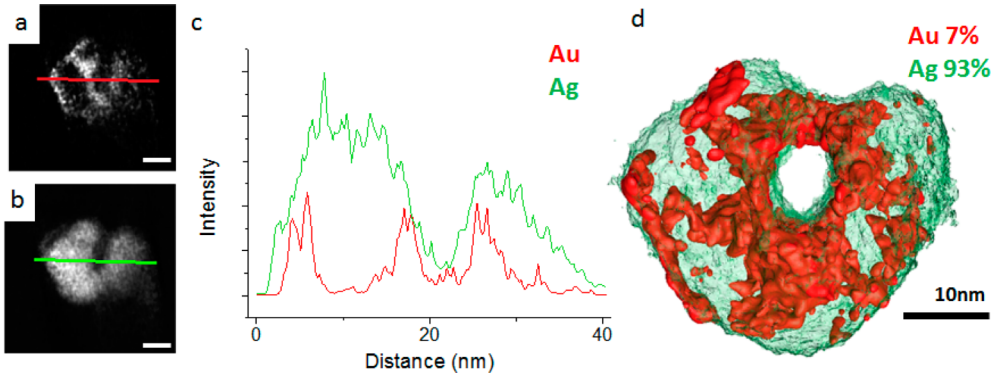

Figure 4. EDX tomogram of nanoparticle with average composition $Ag_{93}Au_7$ with linescan. (a) Au and (b) Ag slices through the respective tomograms. Surface segregation of Au can be seen in the slice through the Au tomogram. (c) Linescan through slices a and b showing the distribution of Ag and Au. Surface segregation of Au is observed although there appears to be a thin surface of Ag outside of the Au. (d) Surface visualization of the Au (red) and Ag (green) tomograms displaying the surface segregation of Au. The scale bars in a and b are 10 nm.

profile from the tomogram (Figure 3f) reveals the benefit of the three-dimensional data set for nanoparticle surface analysis, more clearly demonstrating the segregated surface compared to the profiles obtained from the two-dimensional data (Figure 3c). This is due to the improved resolution in the *z*-direction of the three-dimensional data, removing the contribution of the top and bottom surfaces from the line profile data. Processing of the EDX sum spectrum revealed an average composition of $Ag_{60}Au_{40}$ for the particle shown in Figure 3, close to the average composition of the whole sample ($Ag_{66}Au_{34}$). Figure 3f shows a surface visualization of the Au and Ag tomograms together, which clearly demonstrate the surface segregation of Ag (see Supporting Video S1 for a rotating 3D render). In contrast, the tomogram of a nanoparticle taken from the low Au sample $Ag_{93}Au_7$ shows clear evidence of a thinner (~1 nm) nonuniform Au surface segregation present on both the inner and outer surfaces of the hollow particle (Figure 4) (see Supporting Video S2 for a rotating 3D render).

The 2D compositional mapping and 3D tomographic data show a clear inversion in the surface composition for these particles as the Au content is increased and is in broad agreement with XPS data for large ensembles of nanoparticles (see the Supporting Information). Previous theoretical and lower spatial resolution experimental studies have suggested that particles are either homogeneously alloyed (due to the lower Ag–Au bond energy compared to either Au–Au or Ag–Ag[6,7,26,27]) or have Ag segregated to the surface as a result of this element's lower surface energy.[28]

Our results demonstrate that the Ag and Au distribution in the nanoparticles strongly depends upon the composition of the particle. At low Au content (<18 at. %) galvanic replacement initially proceeds to give Au substitution for Ag at the surface, forming a noncontinuous Au coating. As more Ag is replaced by Au, there is an increased driving force to minimize the particle's intermetallic bond energy and surface energy which produces alloying and finally, at higher concentrations of Au, Ag surface segregation. The maximum catalytic yield is observed at 18 at. % Au, close to the point at which the particles change from Au surface segregation to a homogeneously alloyed composition (Figure 2e). This is consistent with the observation that Au provides a greater yield than Ag for A^3 coupling reactions.[29] It is feasible that the greater electronegativity of Au compared to Ag allows electrons to be transferred from Ag to Au, increasing the electron density of the surface relative to that which would be found in either Ag or Au monometallic systems and improving C–H bond activation of alkynes. Indeed, an XPS analysis of the nanoparticles (Supporting Information, figure and table) revealed that the surfaces of the nanoparticles are enriched in Au relative to their bulk. Moreover, the Au 4f core level binding energy of the materials with the lowest Au content (7 and 18 at. % Au) was found to be somewhat reduced relative to that at higher Au contents (Supporting Information, table), supporting the view that Au is present in ultrasmall metallic aggregates with electronic structure different from metallic bulk Au.[30−32] The Au 4f binding energy of the catalytically most active sample (18 at. % Au) is intermediate (83.44 eV) between those of the most dilute (83.21 eV) and the more Au-rich alloys (83.66 and 83.69 eV), suggesting that high activity is associated with achieving the right balance between the influence of small particle and bulk electronic structure effects. The Ag 3d binding energies detected by XPS vary only slightly and are in the range expected for metallic Ag and its alloys with Au.[33−35]

Our results provide direct 3D observation of an inversion in the segregation of silver and gold for the first time. This approach is not confined to galvanic replacement reactions but could be applied to nanomaterials synthesized via many other chemical and physical processing routes. There are other examples of bimetallic systems which have shown a peak in catalytic performance for a specific composition. In the absence of suitable local compositional information a peak in mass specific activity has been attributed solely to a change in the bulk composition of the nanoparticle.[36] Our results demonstrate that segregation in bimetallic particles is influenced by the synthetic route and is not simple to predict. Furthermore, the experimental results from this study provide direct experimental evidence that nanoscale surface segregation can influence nanoparticle properties. The approach could be extended to analyze the significance of different shape geometries and the facet dependence of enrichment, providing insights for the improved design and understanding of nanoparticle synthesis and catalytic activities.

■ ASSOCIATED CONTENT

Supporting Information

Details of synthesis, the catalysis of the three-component coupling-reaction, STEM imaging, tomography and XPS analysis; figures demonstrating the single/polycrystalline nature of nanoparticles, EDX spectra, and XPS spectra; and videos of aligned tilt series and rotating views of isosurface renders. This

dx.doi.org/10.1021/nl4047448 | *Nano Lett.* 2014, 14, 1921−1926

material is available free of charge via the Internet at http://pubs.acs.org.

AUTHOR INFORMATION

Corresponding Authors

*E-mail: sarah.haigh@manchester.ac.uk.
*E-mail: camargo@iq.usp.br.

Author Contributions

P.H.C.C. and A.M. synthesized the nanoparticles, performed preliminary TEM imaging, and measured catalytic data. T.J.A.S. and S.J.H. performed the STEM imaging and EDX analysis and wrote the paper. T.J.A.S. performed the 3D reconstructions. S.L.M.S. performed the XPS measurements and data analysis. All authors contributed to the interpretation and commented on the manuscript.

Notes

The authors declare no competing financial interest.

ACKNOWLEDGMENTS

T.J.A.S., P.O.B., and S.J.H. thank the UK Engineering and Physical Sciences Research Council, NowNANO doctoral training centre for funding support. S.J.H. thanks the USA Defense Threat Reduction Agency (grant number HDTRA1-12-1-0013) and Gates Foundation for funding support. P.H.C.C. and A.M. thank FAPESP and CNPq for funding support (grant numbers 2011/06847-0, 2013/19861-6, and 471245/2012-7, respectively). The authors wish to acknowledge the support from HM Government (UK) for the provision of the funds for the FEI Titan G2 80-200 S/TEM associated with research capability of the Nuclear Advanced Manufacturing Research Centre.

ABBREVIATIONS

EDX, energy dispersive X-ray; STEM, scanning transmission electron microscope; HAADF, high-angle annular dark field; EFTEM, energy filtered transmission electron microscopy; XPS, X-ray photoelectron spectroscopy

REFERENCES

(1) Herzing, A. A.; Kiely, C. J.; Carley, A. F.; Landon, P.; Hutchings, G. J. Identification of active gold nanoclusters on iron oxide supports for CO oxidation. *Science* **2008**, *321* (5894), 1331−1335.

(2) Kim, S. W.; Kim, M.; Lee, W. Y.; Hyeon, T. Fabrication of hollow palladium spheres and their successful application to the recyclable heterogeneous catalyst for Suzuki coupling reactions. *J. Am. Chem. Soc.* **2002**, *124*, 7642−7643.

(3) Lou, X. W.; Archer, L. A.; Yang, Z. C. Hollow Micro-/Nanostructures: Synthesis and Applications. *Adv. Mater.* **2008**, *20* (21), 3987−4019.

(4) Sankar, M.; Dimitratos, N.; Miedziak, P. J.; Wells, P. P.; Kiely, C. J.; Hutchings, G. J. Designing bimetallic catalysts for a green and sustainable future. *Chem. Soc. Rev.* **2012**, *41* (24), 8099−8139.

(5) Toshima, N.; Yonezawa, T. Bimetallic nanoparticles - novel materials for chemical and physical applications. *New J. Chem.* **1998**, *22* (11), 1179−1201.

(6) Petri, M. V.; Ando, R. A.; Camargo, P. H. C. Tailoring the structure, composition, optical properties and catalytic activity of Ag-Au nanoparticles by the galvanic replacement reaction. *Chem. Phys. Lett.* **2012**, *531*, 188−192.

(7) Sun, Y. G.; Xia, Y. N. Mechanistic study on the replacement reaction between silver nanostructures and chloroauric acid in aqueous medium. *J. Am. Chem. Soc.* **2004**, *126* (12), 3892−3901.

(8) Skrabalak, S. E.; Chen, J.; Sun, Y.; Lu, X.; Au, L.; Cobley, C. M.; Xia, Y. Gold Nanocages: Synthesis, Properties, and Applications. *Acc. Chem. Res.* **2008**, *41* (12), 1587−1595.

(9) Kim, Y.; Hong, J. W.; Lee, Y. W.; Kim, M.; Kim, D.; Yun, W. S.; Han, S. W. Synthesis of AuPt Heteronanostructures with Enhanced Electrocatalytic Activity toward Oxygen Reduction. *Angew. Chem., Int. Ed.* **2010**, *49* (52), 10197−10201.

(10) Bracey, C. L.; Ellis, P. R.; Hutchings, G. J. Application of copper-gold alloys in catalysis: current status and future perspectives. *Chem. Soc. Rev.* **2009**, *38* (8), 2231−2243.

(11) Cobley, C. M.; Xia, Y. Engineering the properties of metal nanostructures via galvanic replacement reactions. *Mater. Sci. Eng. R-Rep.* **2010**, *70* (3−6), 44−62.

(12) Sun, Y. G.; Xia, Y. N. Alloying and dealloying processes involved in the preparation of metal nanoshells through a galvanic replacement reaction. *Nano Lett.* **2003**, *3* (11), 1569−1572.

(13) Miura, M.; Enna, M.; Okuro, K.; Nomura, M. Copper-catalyzed reaction of terminal alkynes with nitrones − selective synthesis of 1-aza-1-buten-3-yne and 2-azetidinone derivatives. *J. Org. Chem.* **1995**, *60* (16), 4999−5004.

(14) Jenmalm, A.; Berts, W.; Li, Y. L.; Luthman, K.; Csoregh, I.; Hacksell, U. Stereoselective epoxidation of phe-gly and phe-phe vinyl isosteres. *J. Org. Chem.* **1994**, *59* (5), 1139−1148.

(15) Gonzalez-Bejar, M.; Peters, K.; Hallett-Tapley, G. L.; Grenier, M.; Scaiano, J. C. Rapid one-pot propargylamine synthesis by plasmon mediated catalysis with gold nanoparticles on ZnO under ambient conditions. *Chem. Commun.* **2013**, *49* (17), 1732−1734.

(16) Kidwai, M.; Bansal, V.; Kumar, A.; Mozumdar, S. The first Au-nanoparticles catalyzed green synthesis of propargylamines via a three-component coupling reaction of aldehyde, alkyne and amine. *Green Chem.* **2007**, *9* (7), 742−745.

(17) Cui, C.; Gan, L.; Heggen, M.; Rudi, S.; Strasser, P. Compositional segregation in shaped Pt alloy nanoparticles and their structural behaviour during electrocatalysis. *Nat. Mater.* **2013**, *12* (8), 765−771.

(18) Stamenkovic, V. R.; Mun, B. S.; Arenz, M.; Mayrhofer, K. J. J.; Lucas, C. A.; Wang, G.; Ross, P. N.; Markovic, N. M. Trends in electrocatalysis on extended and nanoscale Pt-bimetallic alloy surfaces. *Nat. Mater.* **2007**, *6* (3), 241−247.

(19) Chen, D. H.; Chen, C. J. Formation and characterization of Au-Ag bimetallic nanoparticles in water-in-oil microemulsions. *J. Mater. Chem.* **2002**, *12* (5), 1557−1562.

(20) Wang, A. Q.; Chang, C. M.; Mou, C. Y. Evolution of catalytic activity of Au-Ag bimetallic nanoparticles on mesoporous support for CO oxidation. *J. Phys. Chem. B* **2005**, *109* (40), 18860−18867.

(21) Muller, D. A. Structure and bonding at the atomic scale by scanning transmission electron microscopy. *Nat. Mater.* **2009**, *8* (4), 263−270.

(22) D'Alfonso, A. J.; Freitag, B.; Klenov, D.; Allen, L. J. Atomic-resolution chemical mapping using energy-dispersive X-ray spectroscopy. *Phys. Rev. B* **2010**, *81* (10), 100101.

(23) Midgley, P. A.; Dunin-Borkowski, R. E. Electron tomography and holography in materials science. *Nat. Mater.* **2009**, *8* (4), 271−280.

(24) Mobus, G.; Doole, R. C.; Inkson, B. J. Spectroscopic electron tomography. *Ultramicroscopy* **2003**, *96* (3−4), 433−451.

(25) Genc, A.; Kovarik, L.; Gu, M.; Cheng, H.; Plachinda, P.; Pullan, L.; Freitag, B.; Wang, C. XEDS STEM tomography for 3D chemical characterization of nanoscale particles. *Ultramicroscopy* **2013**, *131* (0), 24−32.

(26) Deng, L.; Hu, W.; Deng, H.; Xiao, S.; Tang, J. Au-Ag Bimetallic Nanoparticles: Surface Segregation and Atomic-Scale Structure. *J. Phys. Chem. C* **2011**, *115* (23), 11355−11363.

(27) Wei, L. Y.; Qi, W. H.; Huang, B. Y.; Wang, M. P. Surface segregation of Au-Ag bimetallic nanowires. *Comput. Mater. Sci.* **2013**, *69*, 374−380.

(28) Gong, H. R. Electronic structures and related properties of Ag-Au bulks and surfaces. *Mater. Chem. Phys.* **2010**, *123* (1), 326−330.

(29) Huang, B.; Yao, X.; Li, C.-J. Diastereoselective synthesis of alpha-oxyamines via gold-, silver- and copper-catalyzed, three-component couplings of alpha-oxyaldehydes, alkynes, and amines in water. *Adv. Synth. Catal.* **2006**, *348* (12−13), 1528−1532.
(30) Radnik, J.; Mohr, C.; Claus, P. On the origin of binding energy shifts of core levels of supported gold nanoparticles and dependence of pretreatment and material synthesis. *Phys. Chem. Chem. Phys.* **2003**, *5*, 172−177.
(31) Willneff, E. A.; Braun, S.; Rosenthal, D.; Bluhm, H.; Hävecker, M.; Kleimenov, E.; Knop-Gericke, A.; Schlögl, R.; Schroeder, S. L. M. Dynamic electronic structure of a Au/TiO_2 catalyst under reaction conditions. *J. Am. Chem. Soc.* **2006**, *128*, 12052−12053.
(32) Mason, M. G. Electronic Structure of Supported Small Metal Clusters. *Phys. Rev. B* **1983**, *27*, 748−762.
(33) Tyson, C. C.; Bzowski, A.; Kristof, P.; Kuhn, M.; Sammy-Naiken, R.; Sham, T. K. Charge Redistribution in Au-Ag Alloys from a Local Perspective. *Phys. Rev. B* **1992**, *45*, 8924−8928.
(34) Bzowski, A.; Kuhn, M.; Sham, T. K.; Rodriguez, J. A.; Hrbek, J. Electronic structure of Au-Ag bimetallics: Surface alloying on Ru(001). *Phys. Rev. B* **1999**, *59*, 13379−13393.
(35) Seah, M. P.; Gilmore, L. S.; Beamson, G. XPS: Binding energy calibration of electron spectrometers 5 - Re-evaluation of the reference energies. *Surf. Interface Anal.* **1998**, *26*, 642−649.
(36) Zhang, H.; Jin, M. S.; Wang, J. G.; Li, W. Y.; Camargo, P. H. C.; Kim, M. J.; Yang, D. R.; Xie, Z. X.; Xia, Y. A. Synthesis of Pd-Pt Bimetallic Nanocrystals with a Concave Structure through a Bromide-Induced Galvanic Replacement Reaction. *J. Am. Chem. Soc.* **2011**, *133* (15), 6078−6089.